Modelling and experimental validation of a compliant under-actuated parallel kinematic manipulator

Nan Ma, Xin Dong, and Dragos Axinte

***Abstract*—Parallel kinematic manipulators (PKMs) are increasingly used in a wide range of industrial applications due to the characteristics of high-accuracy and compact structure. However, most of the existing PKMs are structured with heavy actuators and high stiffness. In this respect, this paper proses a simple, yet effective, parallel manipulator that distinguishes itself through: (1) under-actuation: it employs only a single motor and a driving cable to actuate its three legs; (2) novel foot location: it uses a smart shape memory alloy (SMA) clutch-based driving system (SCBDS) which catches/releases the driving cable, thus, making possible the robot under-actuation; (3) adjustable compliance: its double compliant joints on each limb with a stiffness-adjustable section which renders a safe human-robotic interaction. To support and predict the performance of this under-actuated compliant manipulator, a novel kinetostatic model was developed by considering the generalized internal loads (i.e. force and moment) in three compliant limbs and the external loads on the upper platform. Finally, based on the physical prototype, a set of experiments were conducted to validate the model proposed in this paper. It was found that the proposed kinetostatic model can be validated with the average deviations of 1.8% in position and 2.8% in orientation respectively. Further, the workspace of the system (e.g. discrete and continuous workspace) was studied when different actuating strategies were employed, thus emphasizing the advantages and the limitations of this novel system.**

***Index Terms*-Compliant PKM, under-actuated mechanism, kinetostatic modelling**

I. Introduction

In recent years, PKMs have been increasingly used for rapid positioning and high-precision manufacturing, due to their lightweight, compact structure, high stiffness and accuracy [1,2]. However, most of the PKMs are structured with rigid links and joints, requiring high manufacturing tolerance and complex control algorithms [3,4]. Also, the stiffness of the parallel kinematic system, composed of rigid parts, can be regarded as infinite, leading to the potential risk to the operators during the human-robot interaction [5,6,7].

Up to now, significant efforts have been made for developing novel compliant mechanisms (i.e. continuum robots [8,9,10] and compliant PKMs [11,12]) to satisfy the requirements of industrial and healthcare applications [5,13]. For example, a 6-DoF PKM was developed [14], which is composed of three pairs of notched flexure-based limbs. However, the workspace of the system was restricted by the small strokes of the 2-DoF compliant joints. In order to increase the workspace, a new concept of compliant PKM was proposed to use a fully compliant rod in the PKM [15,16], which can provide larger stroke and better scalability. Further, pneumatic actuators were utilised to construct a fully compliant PKM [17], which could achieve a 6-DoF motion by controlling the length of six limbs. Unlike the PKMs with rigid joints, these compliant robots are fully compliant resulting in a reduction of their stiffness, so significant deviations could be generated if a load is applied at the end effector. Therefore, an approach for building PKM with an appropriate stiffness and workspace needs to be developed for safe human-robot interaction operations.

Also relevant for PKMs, different actuation methods have been studied in last decades: conventional (e.g. electrical motors [10], hydraulics [18], pneumatics actuators [3]) and unconventional (e.g. electromagnetic actuators [19], piezoelectric materials [20]) approaches. Generally speaking, integrating a single actuator for each limb can make the PKM system precise and all the limb lengths vary simultaneously. However, in some applications, this could be less a priority in comparison with an under-actuated system, which would rely on the successive actuation of each limb. One example is the solar panel of satellites, where the panel orientation is repeatedly adjusted in a fixed interval to point it to the light/sun. By using our new design, one motor can control the multi-DoF of end-effector with the successive actuation of each limb to reduce the overall weight of the system. For most of these systems, clutch mechanisms (e.g. electromagnetic) are adopted to switch the states of limbs (i.e. between active and passive), enabling the reduction of the number of actuators for a conventional fully-actuated system [21]. However, as a new material with a high power/weight ratio, shape memory alloy has a great potential to miniaturize the size and weight of the clutch systems. For example, SMA wires were used in a bat-like flapping robots [22,23], where the wing shapes were controlled by the length of the SMA wires by adjusting the current; also SMA wire-based rotational joints [24,25,26] were developed to demonstrate the possibility for adopting this smart material as actuators, where the rotation of joints was directly controlled by adjusting the strain of the SMA wires. To the best knowledge of authors, no research has demonstrated using shape memory alloy actuated mechanism for minimizing the number of actuators and the weight of PKM.

Further, in order to precisely control PKMs, many studied have been focused on the kinematic modelling of conventional rigid-link structures. However, if compliant rods are integrated as limbs or joints, the kinematic behaviour of the overall system needs to be further studied. Up to now, different compliant rod-based mechanisms have been developed and the corresponding kinematic models were established with the consideration of the flexible rod behaviours. For example, a continuum robot was studied [27], in which the flexible rods were regarded as a compliant joint that bends as a pure circular arc for establishing the static equation of the system. A concentric-tube continuum robot [28] was developed and studied for minimally invasive surgery, where the model was established by considering the geometrically exact behaviour of each tube (i.e. pure bending) under the given external loads. Further, the model of a

N. Ma, X. Dong, and D. Axinte are with the Department of Mechanical, Materials and Manufacturing Engineering, University of Nottingham, Nottingham NG7 2RD, U.K. (e-mail: Nan.Ma@nottingham.ac.uk, Xin.Dong@nottingham.ac.uk, Dragos.Axinte@nottingham.ac.uk)

concentric-tube robot that considers the bending and rotation of each tube were derived [29] to improve the kinematic accuracy. Besides, long compliant rods were utilized as limbs to connect the base and upper platform and the cosserat rod theory was adopted to build the overall model of the system [16,30]. Up to now, to the best knowledge of authors, most of the researches adopted the rigid-body-model method to predict the kinematics behaviour of compliant joints (i.e. joints were regarded as pure bending with constant curvature), while the cosserat theory has not been utilized (i.e. joints were regarded as rods with varying curvature, including bending and torsion) in compliant parallel mechanism to improve the modelling accuracy.

To address the aforementioned challenges on modelling the conventional PKMs (e.g. excessive actuators and insecure human-robot interaction), a novel under-actuated 6-DoF PKM, which employs SMA-based clutches to change the state of the limbs (i.e. between the actively actuated and passively locked) to enable the reduction of the number of actuators in the system (i.e. one motor was utilized to actuate the manipulator) is proposed in this paper. Then, the conventional rigid-based joints (i.e. special and universal) of the PKM were replaced by length-adjustable compliant rods to alter the compliance of the system, thus, enabling improved human-robot interaction. After that, a new kinetostatic model of the proposed under-actuated parallel system was established, which considers the overall loads in the system to obtain the position and orientation of the upper platform. At last, after experimentally validating the proposed models, the work volume of the system was calculated and plotted for evaluating the overall performances of the under-actuated PKM.

II. The Design of a Novel Under-Actuated PKM

In this section, a novel under-actuated PKM is introduced (Fig.1), which can achieve multiple-DoF output (i.e. 6-DoF) with a reduced number of actuators for three actuation limbs. For achieving this, the design enables the three free low joints to be driven along tracks with a continuous running cable. The position of the leg along the track depends on the movement of a clutch connected to the lower joint by catching the actuating cable that runs in a closed-loop around the base platform. This might resemble the concept of a ski lift: a driving cable is caught by clutches thus, enabling the transportation of the people along a pre-defined track. With such a generic concept, it is possible to use one motor and a continuous cable to control the movements of multi legs on a predefined line (i.e. track/guide) of a parallel manipulator.

To materialize this idea, a novel SMA wire-based clutch was designed to engage/disengage with a continuous (closed-loop) cable, which is used to change the state (i.e. move or stop) of each leg of PKM on a placing line (Fig.1 (a)). In this paper, we define the assembly of a linear guide and its SMA clutch as one placing line (Fig.1 (e)). Specifically, the continuous cable is circumferentially arranged around a triangular table/base with guides provided by four fixed pulleys and one movable pulley, which is used to drive the independent motions of three clutches with only one motor. A spring (Fig.1 (a)) is connected to the movable pulley to maintain the tension of the cable. The motor is mounted on the movable pulley to drive the cable.

Then, a 6-DoF fully elastic rod-based parallel mechanism (Fig.1 (b)) was developed with its feet/lower joints (i.e. *A*, *B* and *C* in Fig.1 (b)) connected to the proposed SMA clutch-based driving system, so that the PKM is setup. With the movement of the feet (*A*, *B* and *C*) along the placing lines, the pose of the PKM platform will change. Further, in order to actively adjust the performance (i.e. stiffness and stability) of the proposed mechanism, we propose here for the leg design a combination of infinitely stiff and compliant sections (i.e. detail structure shown as Fig.1 (f)). Thus, a new compliant limb with length-adjustable rods (Fig.1 (d)) was developed to construct the stiffness-adjustable parallel mechanism. The three moveable feet, which are mounted on the placing lines respectively, are driven along with linear guides by the closed-loop cable to control the configuration of the system (Fig.1 (e)).

Finally, the overall parallel mechanism, which is composed of the SCBDS and parallel mechanism, is obtained (Fig.1 (e)). Specifically, the ends of the three limbs (i.e. *A*, *B* and *C* in Fig.1 (d)) are mounted on the corresponding three SMA clutches respectively (i.e. *A*, *B* and *C* in Fig.1 (a)), where the positions of three placing lines can be independently controlled (i.e. engaging or disengaging with the driving cable) to change the configuration of the upper platform of the manipulator.

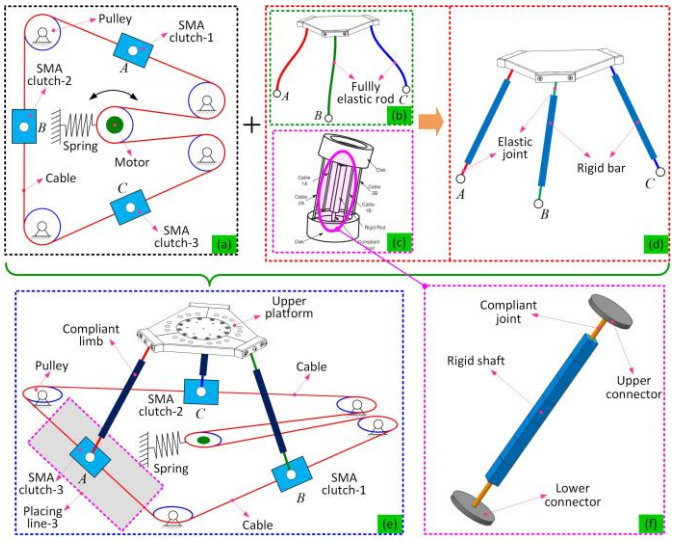

Fig.1. The evolution of the concept of under-actuated PKM. a) schematic diagram of the triangle table with three placing lines to achieve the motion of each leg with only one actuator/motor; b) fully elastic rod-based parallel mechanism with three limbs; c) previously developed concept for constructing the snake arm robot in our group; d) stiffness-adjustable parallel mechanism with compliant joints; e) overall schematic design of the system (i.e. integrates the placing table and parallel mechanism).

As a result, the configuration of the proposed parallel mechanism (i.e. position and configuration of the upper platform in Fig.1 (e)) can be planned in sets of a discrete and continuous succession of poses by utilizing different working algorithms of three placing lines in SCBDS, aspect which will be discussed later. Some of the poses can be achieved by moving continuously all the three placing lines, while other poses only one or two placing lines can be moved at a time. Thus, by employing the aforementioned actuation method of the placing lines, a set of poses of the upper platform can be obtained to perform the given tasks. In addition, it has to be mentioned that the workspace of the upper platform (on which an end-effector/workpiece could be set) is largely decided by the arrangement of three placing lines and characteristics of compliant joints, which is necessary to be ascertained by establishing the kinematic model of the system.

A. *Design of the compliant under-actuated PKM*

The generic concept of the 6-DoF under-actuated parallel mechanism (i.e. 3 active DoFs and 3 passive DoFs at upper

platform), which uses one motor to drive the entire system and a novel SMA wire-based clutch that catches/releases the limbs from the driving cable, is presented in this paper. For each of the limbs, the stiffness-adjustable compliant joints were employed to connect the upper platform and the SCBDS. For this, a rigid bar with a central hole, through which the elastic rod runs, is employed to separate the full length of the leg of the manipulator into two compliant universal joints and a rigid link (Fig.1 (f)). These compliant joints provide the rotation motion between the adjacent parts, which can be regarded as conventional rigid universal joints for calculating the kinematic. As the motion behaviour (i.e. bending angle, rotation centre, maximum stress) of the compliant joint is determined by its length, for this 6-DoF parallel mechanism, a structure of the leg that allows the adjustment of the length of the compliant joint has been adopted. Thus, the rigid bar on the long elastic rod (i.e. two ends of elastic rod are connected with base and upper platform respectively) is combined with several small rigid segments, which allows easy adjustment of the length of the rigid part in the limb, and further to vary the length of the compliant joints at the ends of each limb (i.e. l_0 to l_6 in Fig.2 (c)). Since the overall length of the limb is designed as fixed in this paper, the length of the compliant joint can be varied by increasing/decreasing the number of the rigid bar segments.

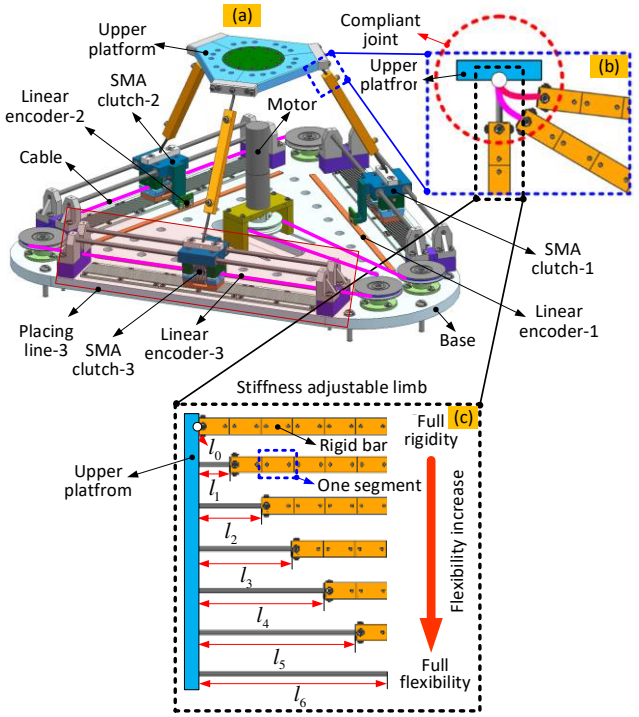

Fig.2. Design of the under-actuated PKM. a) design and motion characteristics illustration of three feet; b) motion characteristic illustration of the compliant universal joint; c) working principle illustration of the stiffness adjustable limb

By combining the proposed parallel mechanism and SCBDS, the overall under-actuated PKM was developed (Fig.2), where three compliant limbs (i.e. detailed structure and working principle shown as Fig.2 (b)) were utilized to connect the placing table and upper platform. In order to conveniently adjust the length of compliant joints for actively changing the performance of the system (i.e. stiffness and stability), the length adjustable limb was designed (Fig.2 (c)). Thus, six compliant joints made of super-elastic Nitinol, which could be considered kinematically equivalent as universal joints, provide the rotation motion for the upper platform. In addition, a feedback system (i.e. linear encoder) was employed on each placing line for the closed-loop control.

B. Design of the SMA clutch-based driving system

The key element to enable the SMA clutch-based driving system is a clutch that is "on" when the limb needs to catch the driving cable to move along the guide and "off" when the limb needs to retain a stable position. Based on this working principle (Fig.1), a novel design of SMA-wire based clutch was proposed, enabling to move and retain each limb in an independent way with only one actuator (i.e. motor).

For the use of an under-actuated PKM, the miniaturized clutch needs to fulfil the following main requirements: i) appropriate working stability to perform reliable clamping and releasing of the placing line to the base platform; ii) be small and light for optimizing the size and weight of the driving system; iii) provide two independent working functions, i.e. engage/disengage with the moving cable to move/stop the limbs separately. Based on the abovementioned requirements, an SMA wire, which can adjust its length once its temperature is varied, was selected as the actuator of the clutch.

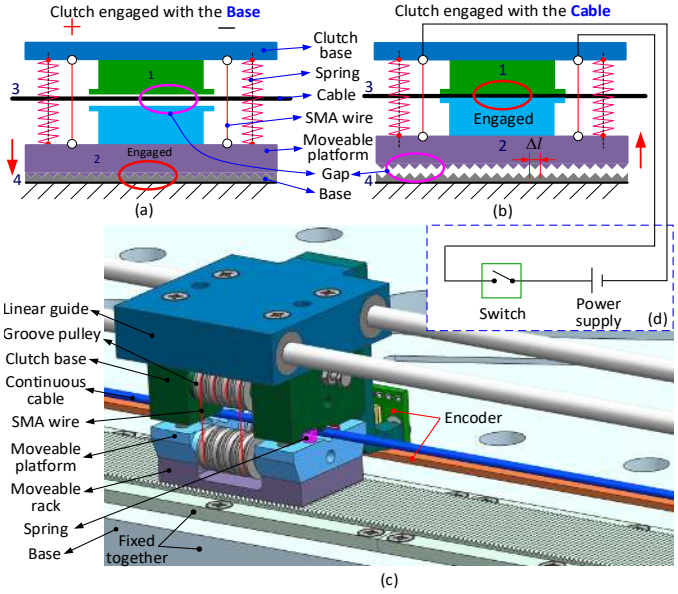

Fig.3. Concept and working principle of the proposed SMA wire-based clutch. a) clutch engaged with the base; b) clutch engaged with the cable; c) design of SMA clutch and winding of SMA wire; d) control schematic for SMA clutch

The working principle of the clutch is shown as follows: when the SMA is heated up by applying a current, the movable platform of the clutch (green part – Fig.3, numbered 2) engages with the clutch base (4) and clamps the cable (3), so the whole clutch moves with the driving cable (Fig.3 (b)); when the SMA wire is cooled down by switching off the current and it stretched back to its original length, the moveable platform (2) engages with the base (4) and disengages with the cable (3) in Fig.3 (a). In order to lock the SMA clutch once it reaches the desired position, saw tooth tracks on the base and moveable platform were employed to ensure that a foot keeps its location after being placed along with the linear guide. As the sawtooth was adopted to increase the locating stability, the resolution of placing lines, Δ_l, was decided by the pitch of sawtooth.

The structure design of the SMA clutch is shown in Fig.3 (c). In order to reduce the friction of the SMA wire winded on SMA clutch, miniature groove pulleys (Fig.3 (c)) have been employed to guide the motion of SMA wire. When a current is applied to the SMA wire (switch "on" - Fig.3 (d)), the moveable

platform and rack will be pulled up together against the driving cable, so the linear guide will be engaged with the motor. When the switch is "off", the moveable platform will be pushed back by the spring to be engaged with the toothed track while disconnecting with the driving cable.

Based on this concept of the SMA wire-based clutch, the entire SMA clutch-based driving system for the under-actuated PKM was developed (Fig.4). In the design example of the SCBDS, three identical placing lines are located at three sides of a triangle base plate, while the motions are actuated by a single motor located at the centre of triangle plate. In this design, the SMA wire-based clutch can move together with the driving cable when the clutch is engaged with the cable (clutch is on); while it stops when the clutch is engaged with the table (clutch is off). For achieving the better positioning performance of placing lines, the position sensors (i.e. linear encoder and magnetic scale mounted on SMA clutch and system base respectively, Fig.4) are included for closed-loop control of the position of the clutch.

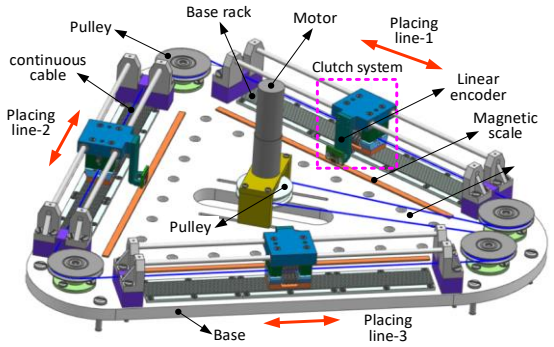

Fig.4. The design of the SMA clutch-based driving system that enables the under-actuation of the compliant parallel manipulator (here not presented)

In this section, the novel parallel mechanism and SCBDS were combined to construct an under-actuated compliant robot for safe human-robot interaction with a reduced number of actuators. Due to the introduction of compliant joints in the proposed parallel mechanism, the kinetostatic model of the compliant joints, as well as for the overall under-actuated system, are required to make the system work. Thus, in the following section, the kinetostatic modelling of the system, which reflects the relationship between the pose of the upper platform and the position of the clutch, is conducted.

III. MODELLING OF THE UNDER-ACTUATED PKM

In this section, we generalised the modelling of the proposed 6-DoF under-actuated parallel mechanism (i.e. 3 active and passive DoFs, respectively), which is composed of three compliant length-adjustable limbs and one SCBDS. Unlike the conventional approaches (e.g. Pseudo-Body-Method and Cosserat-Theory-Method [32,33]), a new kinetostatic model of the proposed manipulator was proposed. This method considers the input loads (i.e. external loads on the upper platform) and the position of the clutch-based driving system to predict the configuration of the system. Also, the new model proposed in this paper aims to describe for the first time the kinetostatic behaviour of an under-actuated PKM. By establishing the parametric static equation of the manipulator, the pose of the upper platform (i.e. position and orientation) can be predicted after giving the positions of three placing lines of the PKM. The model of the under-actuated PKM is derived by two steps: i) kinetostatic model of single compliant limb; ii) kinetostatic model of the entire compliant manipulator.

A. *Kinetostatic modelling of a single compliant limb*

In the proposed manipulator, compliant rods were adopted to replace the conventional universal/spherical joints at the ends of each limb. The new design brings an advantage of safe robot-human interaction. However, it also brings difficulties for specifying the position and orientation of the upper platform (i.e. due to the internal forces generated in the joints and the under-actuated mechanism). Thus, in order to control the manipulator, a kinetostatic model of a single compliant limb, which considers the internal forces caused by the material deformation, is built at first. A flowchart of the overall forward kinetostatic model of the manipulator is shown in Fig.5.

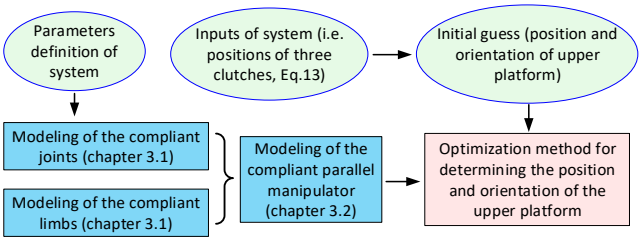

Fig.5. Flowchart of the forward kinematic model of the under-actuated parallel kinematic manipulator

During the operation, the compliant joints can be elastically deformed in several modes (i.e. bending, torsion and shear). Hence, different internal forces (i.e. bending torsion and shear) in the compliant joints are considered to build an accurate model. Thus, the equations of the distal position and orientation, as well as the generated internal forces and moments in limbs, were established for building the statics equations of the system (Fig.6).

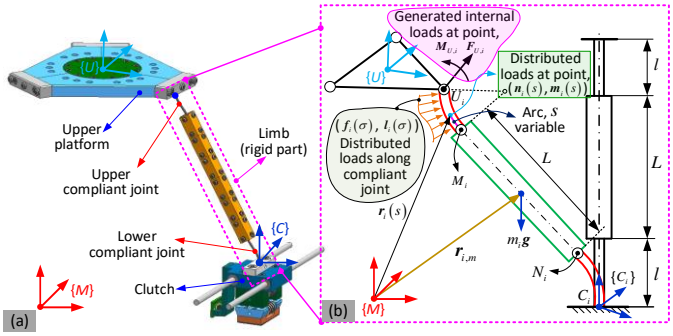

Fig.6. Schematic for kinetostatic modelling (i.e. shape deformation and internal force) of the compliant joint in one arbitrary limb: a) joint assembling principle; b) shape deformation and the kinematic variables of the compliant joint.

The modelling of a single compliant limb is divided into two stages: 1) the development of the static equation of single compliant joint; 2) the derivation of the static equation of the entire limb that has two compliant joints (to link it with upper and lower platforms of the PKM).

Due to the identical structure design, all the limbs share the same motion characteristics. Firstly, one limb (i.e., limb, *i*, in Fig.6 was selected as an example for building the kinetostatic modelling. Then the necessary coordinates were established to study the kinetostatic characteristics of the system, which are the local coordinate $\{M\}$, the coordinate of the upper platform $\{U\}$, the lower joint coordinate of the *i*-th limb $\{C_i\}$.

Step One (modelling single compliant joint, Fig.6): based on the constitutive law of cosserat rod, the limbs can be balanced under the internal (i.e. distributed forces and moments) and external (i.e. forces and moments from tip point) loads at every location along the compliant joint. Thus, the static equation at any arbitrary point can be established as follows:

$$\begin{cases}\mathbf{n}_i(s)=\int_s^{2l+L}\mathbf{f}_i(\sigma)d\sigma+m_i\mathbf{g}\\ \mathbf{m}_i(s)=\mathbf{r}_{i,m}\times m_i\mathbf{g}+\int_s^{2l+L}\left(\mathbf{r}_i(\sigma)\times\mathbf{f}_i(\sigma)+\mathbf{l}_i(\sigma)\right)d\sigma+\mathbf{r}_i(s)\times\mathbf{n}_i(s)\end{cases} \quad (1)$$

Where, $\mathbf{n}_i(s)$ and $\mathbf{m}_i(s)$ are the internal force and moment at point, s, along the compliant joint; l and L are the lengths of the compliant joint and rigid shaft respectively; m_i is the mass of i-th joint; $\mathbf{g}$ is the gravitational acceleration; $\mathbf{r}_{i,m}$ is the position vector of the centroid of the rigid shaft in local coordinate; $\mathbf{f}_i(\sigma)$ and $\mathbf{l}_i(\sigma)$ are the distributed forces and moments in the compliant joint, which were caused by the plastic deformation of the compliant joints; $\mathbf{r}_i(s)$ is the deformed shape vector of at a point, s, of the compliant joint.

Deriving (1) with the arc length, s (the arc length from point s to M_i, Fig.6), the differential equations relating to the distributed force and moment in limb, i, can be obtained.

$$\begin{cases}\dot{\mathbf{n}}_i(s)+\mathbf{f}_i(s)=\mathbf{0}\\ \dot{\mathbf{m}}_i(s)+\mathbf{l}_i(s)+\dot{\mathbf{r}}_i(s)\times\mathbf{n}_i(s)=\mathbf{0}\end{cases} \quad (2)$$

Where, $\dot{\mathbf{n}}_i(s)$ and $\dot{\mathbf{m}}_i(s)$ are the differentials of the force and moment with the length of the limb at point s; $\dot{\mathbf{r}}_i(s)$ is the differential of shape vector at point s.

Further, the internal loads of the compliant joint (i.e., bending and torsion moments that are generated by the material deformation) are expressed by the curvature variation relative to the initial curvature:

$$\mathbf{m}(s)=\mathbf{R}(s)\mathbf{K}(s)\Delta\mathbf{u}(s) \quad (3)$$

Where, $\mathbf{R}(s)\in SO(3)$ is the orientation of the local moving coordinate at point, s, relative to the local fixed reference $\{M\}$; $\mathbf{K}(s)$ is the stiffness matrix of the compliant rod by considering the bending and torsional stiffness respectively; $\Delta\mathbf{u}(s)$ is the variation of the curvature of the compliant joint at point, s, which can be expressed as $\Delta\mathbf{u}(s)=\mathbf{u}(s)-\mathbf{u}^*(s)$. Where, $\mathbf{u}(s)$ is the curvature vector of the compliant joint after deformation, and $\mathbf{u}^*(s)$ is the initial curvature vector. In the design of proposed manipulator, the compliant limbs are directly assembled on the base. Thus, the initial stress-free state of the rod is expressed as $\mathbf{u}_i^*=[0\quad 0\quad 0]^T$.

In order to eliminate the moment variation of (2) in compliant joint, i, the derivative was taken on (3) by the arc length, s.

$$\dot{\mathbf{m}}_i=\mathbf{R}_i\left(\mathbf{K}_i\left(\dot{\mathbf{u}}_i-\dot{\mathbf{u}}_i^*\right)+\mathbf{u}_i^{\wedge}\mathbf{K}_i\left(\mathbf{u}_i-\mathbf{u}_i^*\right)\right) \quad (4)$$

Combining (2) and (4) to eliminate the differential of the moment, $\dot{\mathbf{m}}_i(s)$, the variation of curvature, $\dot{\mathbf{u}}$, related to distributed loads and rod parameters can be established. For simplicity, the detail process in obtaining the derivative of the moment was omitted here [28]. Here, for the simplification, the notation (s) was inputted in the equation.

$$\dot{\mathbf{u}}_i=\dot{\mathbf{u}}_i^*-\mathbf{K}_i^{-1}\left(\left(\dot{\mathbf{u}}_i\mathbf{K}_i+\dot{\mathbf{K}}_i\right)\left(\mathbf{u}_i-\mathbf{u}_i^*\right)+\hat{\mathbf{e}}_3\mathbf{R}_i^T\left(\int_s^l\mathbf{f}_i(\sigma)d\sigma+m_i\mathbf{g}\right)+\mathbf{R}_i^T\mathbf{l}_i\right) \quad (5)$$

The boundary conditions for the compliant limb can be expressed as follows:

$$\mathbf{g}_i(0)=\begin{bmatrix}\mathbf{R}_{C,i} & \mathbf{P}_{C,i}^T\\ \mathbf{0}_{1\times3} & 1\end{bmatrix}$$
$$\mathbf{m}_i(2l+L)=\mathbf{M}_{U,i} \quad (6)$$

Where, $\boldsymbol{R}_{C,i}$ and $\boldsymbol{P}_{C,i}^T$ are the orientation matrix and position vector, respectively, at the initial point (M_i) of the rod related to the assembling characteristic (Fig.6). Thus, (5) allows finding the curvature variation along the compliant limb with the given boundary conditions, (6).

Step Two: for establishing the static equation of the rigid shaft in the i-th limb, the following coordinates were defined, which represent the orientation and position of the compliant joints and rigid shaft: the coordinates $\{\boldsymbol{O}_{U,i}\}$ and $\{\boldsymbol{O}_{C,i}\}$ are located at the tip and end of the compliant limb to define their local moving coordinates (i.e. $\boldsymbol{g}(2l+L)$ and $\boldsymbol{g}(0)$ in (16)) respectively; the coordinates $\{\boldsymbol{O}_{M,i}\}$ and $\{\boldsymbol{O}_{N,i}\}$ are located at the two ends of rigid shaft (i.e. distal and proximal) to define their positions and orientations respectively; the coordinate $\{\boldsymbol{O}_{R,i}\}$ is located at the geometrical centroid of the rigid shaft, which is parallel with $\{\boldsymbol{O}_{M,i}\}$ and $\{\boldsymbol{O}_{N,i}\}$.

Further, considering the mass of the rigid shaft, the variation of the distributed force and moment at two ends of the rigid part of the shaft keep its balance (Fig.7):

$$\begin{cases}\mathbf{f}_i(M_i)=-\mathbf{f}_i(N_i)-m_i\mathbf{g}\\ \mathbf{l}_i(M_i)=-\mathbf{l}_i(N_i)+\mathbf{r}_i(M_i)\times\left(\mathbf{f}_i(N_i)+m_i\mathbf{g}\right)-\mathbf{r}_i(N_i)\times\mathbf{f}_i(N_i)-\mathbf{r}_{i,m}\times m_i\mathbf{g}\end{cases} \quad (7)$$

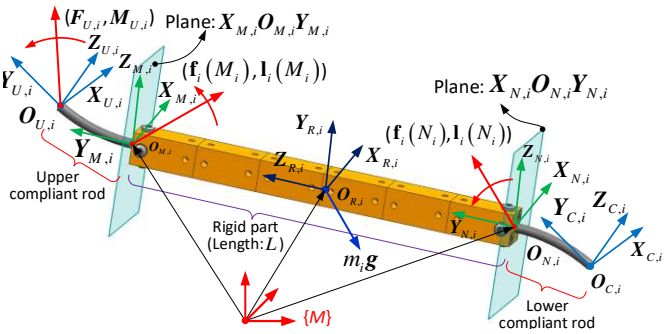

Fig.7. Schematic of the kinematics of the under-actuated PKM

Where, $\boldsymbol{f}_i(M_i)$ and $\boldsymbol{l}_i(M_i)$ are the distributed force and moment at point M_i; $\mathbf{f}_i(N_i)$ and $\mathbf{l}_i(N_i)$ are the distributed force and moment at point N_i; $\boldsymbol{r}_i(M_i)$ and $\boldsymbol{r}_i(N_i)$ are the position vectors of points M_i and N_i in local coordinate $\{M\}$.

After establishing the load-deformation differential equations of a general cosserat rod (i.e. single compliant joint), the kinetostatic model of a single compliant limb (two compliant rods and one rigid shaft) was developed, (7). With the established model, the configuration of the limb can be calculated under any given boundary conditions (i.e., external loads $\mathbf{F}_{U,i}$ and $\mathbf{M}_{U,i}$ in Fig.6. Further, the kinetostatic model of the overall system (constructed by one upper platform and three compliant limbs) can be progressed (the next section).

B. Kinetostatic modelling of the whole system

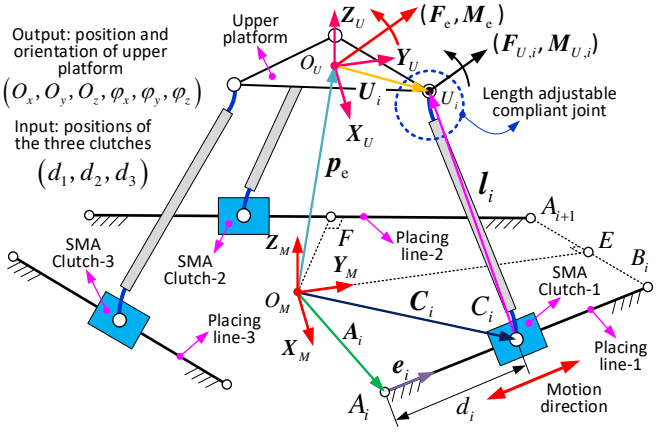

Fig.8. Schematic of the kinematics of the under-actuated PKM

As the proposed compliant PKM is structured with an upper platform and three compliant limbs, the position and orientation of the upper platform is determined by the configurations of the limbs. In this section, with the previously established model of

a single compliant limb, the forward kinetostatic model of the entire system was developed to obtain the pose of the upper platform (i.e. position and orientation) under any given inputs of the SMA clutch-based driving system (i.e. positions of three clutches along the placing lines).

a) Static constraint on the upper platform

For each configuration of the manipulator (i.e. different positions of the SMA clutches along the placing lines), the kinetostatic equations of the upper platform can be obtained (Fig.8). According to the previous research [34,35], the static equation of the compliant parallel manipulators can be established in the form of the force and moment constraints of the upper platform (i.e., from external and internal loads of the compliant joints) (Fig.8).

$$\begin{cases} \sum_{i=1}^{3} \mathbf{F}_{U,i} - \mathbf{F}_e = \mathbf{0} \\ \sum_{i=1}^{3} \mathbf{F}_{U,i} \times \left(\mathbf{R}_U \mathbf{U}_i + \mathbf{p}_e\right) + \sum_{i=1}^{3} \mathbf{M}_{U,i} + \mathbf{F}_e \times \mathbf{p}_e - \mathbf{M}_e = \mathbf{0} \end{cases} \tag{8}$$

Where, $\mathbf{F}_e$ and $\mathbf{M}_e$ are the force and moment on the upper platform, respectively; $\mathbf{F}_{U,i}$ is the internal force in i-th compliant joint; $\mathbf{M}_{U,i}$ is the internal moment of the i-th compliant joint in local coordinate $\{M\}$; $\mathbf{F}_e$ is the external force applied on the upper platform in local coordinate $\{M\}$; $\mathbf{M}_e$ is the external moment of the upper platform in local coordinate $\{M\}$; $\mathbf{R}_U$ is the rotation matrix of the upper platform in local coordinate $\{M\}$; $\mathbf{U}_i$ is the position vector of the i-th joint in upper platform coordinate $\{U\}$; $\mathbf{p}_e$ is the position vector of the upper platform in local coordinate $\{M\}$.

For defining the rotation matrix, $\mathbf{R}_U$, the **ZYX** Euler angle was used to define the orientation of the upper platform. The process can be stated as follows: the upper platform coordinate was originally transformed from point, O_M, in local coordinate $\{M\}$ to point, O_U; then, the upper platform coordinate was rotated around the axes $\mathbf{Z}$, $\mathbf{Y}$ and $\mathbf{X}$ with angles θ_z, θ_y and θ_x, respectively. Thus, the rotation matrix can be expressed as:

$$\mathbf{R}_U = \begin{bmatrix} c\theta_z c\theta_y & c\theta_z s\theta_y s\theta_x - s\theta_z c\theta_x & c\theta_z s\theta_y c\theta_x + s\theta_z s\theta_y \\ s\theta_z c\theta_y & s\theta_z s\theta_y s\theta_x + c\theta_z c\theta_y & s\theta_z s\theta_y c\theta_x - c\theta_z s\theta_x \\ -s\theta_y & c\theta_y s\theta_x & c\theta_y c\theta_x \end{bmatrix} \tag{9}$$

Where, $s\theta = \sin\theta$ and $c\theta = \cos\theta$.

b) Geometrical constraints on compliant limbs

By considering the geometrical constraints, the tip position and orientation of the limb (the upper compliant joint ($\mathbf{O}_{U,i}$, Fig.7)) can be obtained. Thus, the geometrical constraints can be established for ascertaining the configuration of the system.

As the stiffness of the rigid shaft is much higher than the compliant rods, the elastic deformations of the limb were considered to occur at the compliant rods. Thus, the following equations can be established regarding the position and orientations at points $\mathbf{M}_i$ and $\mathbf{N}_i$ based on the geometrical constraints of the rigid shaft.

$$\begin{cases} \mathbf{R}(M_i) = \mathbf{R}(N_i) \\ \mathbf{r}(M_i) = \mathbf{r}(N_i) + \mathbf{R}(N_i)\begin{bmatrix} 0 & 0 & L \end{bmatrix}^T \end{cases} \tag{10}$$

Where, $\mathbf{R}(M_i)$ and $\mathbf{R}(N_i)$ are the attached local moving coordinate of points $\mathbf{M}_i$ and $\mathbf{N}_i$; $\mathbf{r}(M_i)$ and $\mathbf{r}(N_i)$ are the position vectors of attached frames in local coordinate; L is the length of the rigid shaft (Fig.6).

Based on the differential equations (i.e. (5) and (6)) and geometrical constraints ((10)) of the compliant rods and rigid shaft, the position and orientation of the limb tip can be calculated to obtain the geometrical constraints of the PKM.

$$\left[\log\left(\mathbf{R}\left((2l+L)_i\right)^T \mathbf{R}(U_i)\mathbf{R}_{\alpha_i}\right)\right]^{\vee} = \mathbf{0}, \quad i = 1,2,3 \tag{11}$$

Where, log is a natural logarithm of the matrix, which maps $SO(3)$ to $\mathfrak{so}(3)$; $\vee$ denotes the conversion of a matrix from $\mathfrak{so}(3)$ to its corresponding $\mathbb{R}^3$; $\mathbf{R}(U_i)$ is the rotation matrix of the upper platform; $\mathbf{R}_{\alpha_i}$ is the angular displacement vector, which represents the pre-defined offset orientation between the upper platform and assembling vector of the compliant limb. Note: $\mathbb{R}^3$ is the real matrix group; $SO(3)$ and $\mathfrak{so}(3)$ are the special orthogonal and Euclidean groups respectively.

Further, the position vector loop constraint of three compliant limbs (Fig.8) can be expressed ((12)):

$$\mathbf{R}(U_i)\mathbf{U}_i = \mathbf{r}(2l+L) - \mathbf{p}_e, \quad i = 1,\cdots,3 \tag{12}$$

As the three placing lines have fixed orientations on the base platform, the position vector of SMA clutch, $\boldsymbol{C}_i$, in the i-th placing line can be expressed as:

$$\mathbf{C}_i = \mathbf{A}_i + d_i\mathbf{e}_i, \quad i = 1,\cdots,3 \tag{13}$$

Where, $\mathbf{A}_i$ is the position vector of point, A_i, in the global reference; d_i is the distance between SMA clutch and point, A_i; $\mathbf{e}_i$ is the unit vector of the i-th placing line.

Hence, based on the static constraints ((1) to (7)) and the geometric boundary conditions ((10) and (11)) of the compliant limbs, an iteration approach was utilised to find the solutions that satisfy (8), which is the configuration of the upper platform.

Since a novel under-actuated compliant system is presented, a new kinetostatic method for analysing the configuration of the system was introduced, which is different from the conventional approaches (e.g., Pseudo-Body and Cosserat-Theory Methods). This method considers the generated loads (i.e. internal force and moment) of the compliant joints and the under-actuated structure, which can predict the non-circular deflection of the joints. Based on this analysis of the joints, the kinetostatic behaviour of the under-actuated system is described, which can be also utilised for other under-actuated compliant parallel systems.

IV. Experimental Validation and Performance Study

In the previous section, the forward kinetostatic model of the compliant rod-based parallel system was introduced ((8) to (11)). In order to validate the proposed kinetostatic model, a set of experiments were conducted by moving the upper platform by controlling the positions of three clutches along the track of the base platform. In the experiments, the configurations of the upper platform were measured by a vision-based tracking system.

A. Model validation for a single compliant limb

Firstly, the kinematic performances of a single compliant limb were studied under different static load conditions. To validate the proposed model of a limb, one of its ends was mounted while measuring the deflection of the limb when loading the other end (Fig.9). A grid paper was utilized as the background for scaling the limb trajectory during the experiments, which were then compared with the results from the theoretical calculations. Visual measurements were employed for validating the model of a single compliant joint, but the more accurate measurements (i.e. VICON) were adopted for the experiments of the overall system.

As super-elastic NiTi rods were employed to replace the conventional rigid universal joints, the kinetostatic characteristics of the compliant limb were carefully studied

based on the cosserat rod theory. The parameters of the NiTi rods utilized in experiments are shown in Table 1.

Table 1. Structure parameters of compliant limb

Parameters	Rod Length	Rod diameter	Material	Piece length
Value	200 mm	1.0 mm	NiTi	20 mm

With one limb configured as a cantilever beam (Fig.9), the weights with different masses (i.e. 0.29 N and 0.62 N respectively), were hanged at the end of the limb. Then, the kinetostatic modelling of a single compliant limb proposed in the previous section was implemented with the same boundary conditions to calculate the limb trajectories.

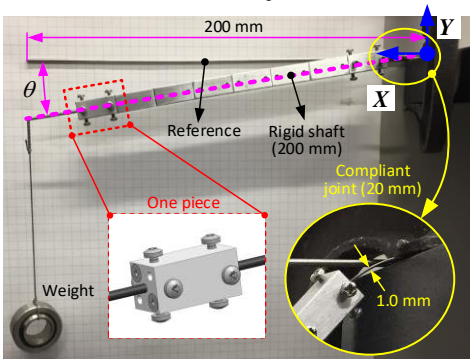

Fig.9. Experimental setup for validating the model for a compliant limb. A compliant limb was tested as a cantilever beam (total length: 200 mm, including two 20 mm long compliant joints and one 160 mm long rigid part).

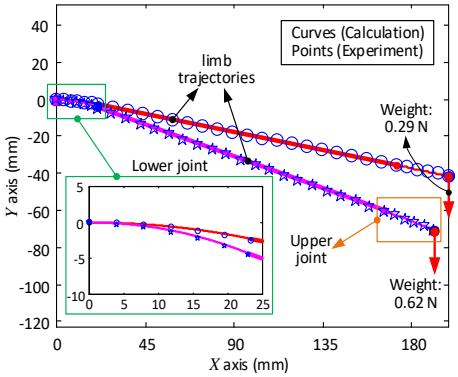

Fig.10. Comparison between modelled and experimental results of the deflections of the compliant limb under different loads.

From Fig.10, it can be seen that the simulation results match those from the experiments (average error: 4.7%) well at the measured points. Under two different loads (i.e., 0.29 N and 0.62 N), the maximum error between the simulation and experimental results are 0.75 mm and 0.87 mm, respectively. The values of the deformations of the compliant joint presented in these tests (Fig.10) are representative that happens during the operation of the PKM. Hence, it can be concluded that the proposed model of a single compliant limb is accurate for predicting the kinetostatic performance of a single leg. Based on the structure design of the PKM, each limb is deformed within 20°, thus the current experiment under 0.29 N and 0.62 N (deformation angles are 12° and 21° respectively) end loads can validate the modelling of a single limb. Then, based on the validated model of a single limb, the model of the entire parallel kinematic system was tested and presented in the following part.

B. Validation of the under-actuated manipulator model

As commented, the under-actuated PKM system proposed here can perform a 6-DoF manipulation, which is actuated by positioning the SMA based clutches along three placing lines using a single driving cable. Thus, the forward kinetostatic model is of key importance to predict the output of the system (i.e. workspace of the upper platform) for given inputs (i.e. positions of three placing lines).

The validation process of the proposed kinetostatic modelling was performed based on the prototyped PKM (Fig.11). After connecting the SMA clutch-based driving system and upper platform by the three same structured complaint limbs (i.e. the ends of limbs are fixed firmly on the clutch and upper platform respectively to avoid the relative rotation during the working of the system), the PKM is configured.

After planning the motion trajectories of three placing lines, the control system was employed to actuate the three placing lines to the desired positions, respectively. Then, the developed kinetostatic model and camera system were used to get the outputs of the upper platform. At last, the results from the two methods were compared and plotted for the model evaluations.

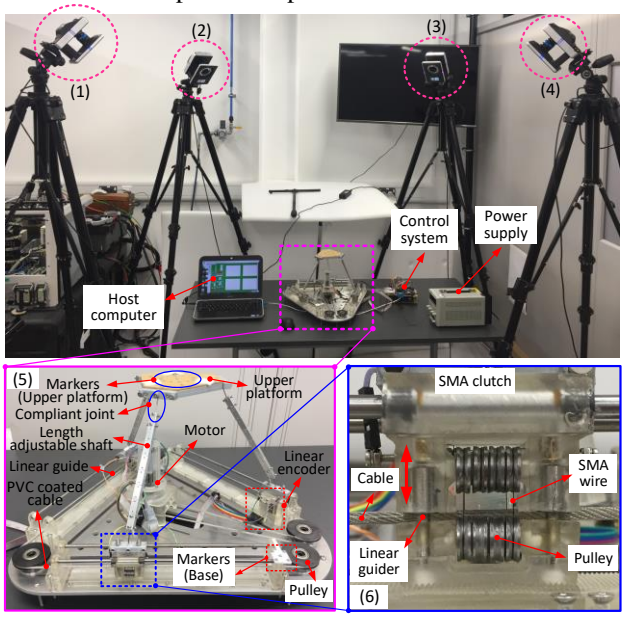

Fig.11. Experimental setup and detailed structure of the compliant parallel manipulator. Note: the motion capture system with four cameras (i.e. (1) to (4)) was employed to evaluate the position and orientation of the upper platform under the given inputs of three placing lines

The experimental setup (Fig.11) includes the under-actuated system (5), a host computer, control system, power supply and a motion capture system ((1) to (4)), VICON (UI-5480VP), that was deployed to measure the position and orientation of the upper platform for the model validation. In the test, two coordinate systems (i.e. the upper platform and base coordinate systems respectively constructed by the corresponding markers) were set up in the camera system. Then, the kinematic models ((8) to (12)) were employed to obtain the configuration of the upper platform in the local coordinate system (Fig.6).

In the manipulator, one motor (Maxon DCX32L) integrated with a gearbox (Maxon GPX32, reduction ratio - 138:1) and encoder (Maxon ENC16 with 1024 pulses) was used to drive a PVC coated cable (i.e. outer diameter: 2.3mm, inner steel wire diameter: 1.5mm). Three identical placing lines, which are composed of SMA clutches, guiding system and linear encoder, are located at the three sides of the triangle base. Then, three linear encoders (receiver: RLC2IC, resolution: 0.244μm) have been used to measure the positions of three placing lines. Based on the properties of SMA wire, the time for each set of

movement of SMA clutch (from one end to another end of stroke) is around 6.2s (i.e. 1s for contracting the SMA wire to clamp the cable, 3.2s for driving the clutch to move and 2s for cooling down the clutch to release the cable).

The control strategy for implementing the clutch-based driving system is shown as Fig.12.

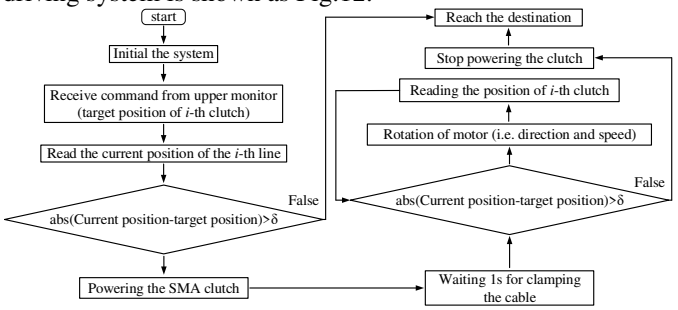

Fig.12. The control strategy for the clutch-based driving system (*i*-th placing line was selected)

The parameters of the prototype are shown in Table 2 (i.e. the parameters are defined based on Fig.8).

Table 2. Prototype parameters for the model validation (Fig.8). Unit: mm

Variables	Variable description	Value (mm)
$\boldsymbol{A}_1$	The vector of point A_1 in {*O*}	[193.7, -64.3, 0]
$\boldsymbol{A}_2$	The vector of point A_2 in {*O*}	[-75.4, 189.5, 0]
$\boldsymbol{A}_3$	The vector of point A_3 in {*O*}	[-140, -148.4, 0]
$\boldsymbol{e}_1$	The unit vector of the moving direction of placing line-1	[-0.42, 0.91, 0]
$\boldsymbol{e}_2$	The unit vector of the moving direction of placing line-2	[-0.42, -0.91, 0]
$\boldsymbol{e}_3$	The unit vector of the moving direction of placing line-3	[1, 0, 0]
$\boldsymbol{U}_1$	The coordinate of the upper compliant joint U_1 in {*U*}	[61.5, 35.5, 0]
$\boldsymbol{U}_2$	The coordinate of the upper compliant joint U_2 in {*U*}	[-61.5, 35.5, 0]
$\boldsymbol{U}_3$	The coordinate of the upper compliant joint U_3 in {*U*}	[0, -71, 0]
d_1,d_2,d_3	Motion stroke of the placing line	[0 ~ 210]

Three different compliant joints (i.e. various joint lengths: 20; 30; 40 mm) have been employed in the experiments to test the validity of the proposed model for a different level of the compliance of the system (Table 3). Thus, for each experiment, the length of the rigid shaft was changed (i.e. by varying the number of rigid pieces in the limb) to adjust the length of the compliant joints (Fig.2), and further to alter the compliance of the PKM.

Two key parameters were varied for validating the kinetostatic model of the entire under-actuated PKM: (i) the positions of the lower joints (given by the position of the clutches); (ii) the compliance of the PKM.

Firstly, the inputs of the three placing lines (i.e. position of the clutches) were planned (Table 3) based on which, by using the forward kinematics, the corresponding configurations of the upper platform were evaluated while the experimental data was captured by the camera system. This enabled the comparison of the simulated and experimental results.

Table 3. Positions of the placing lines (inputs) for the validation of the model determining the position and orientation of the upper platform (outputs)

Test number	1	2	3	4	5	6	7	8	9	10	11	12
Placing Line 1 (mm)	0	0	0	40	40	40	80	80	80	120	120	120
Placing Line 2 (mm)	40	40	80	0	0	80	0	0	40	0	0	40
Placing Line 3 (mm)	80	120	120	80	120	120	40	120	120	40	80	80

For a better understanding of the behaviour of the system when varying the length of compliant joints (Table.3), the configurations of the upper platform were measured under different lengths of the compliant joints (i.e. 20, 30 and 40 mm, respectively). Here, as the base for discussions, three groups of the experiments (i.e. number 3, 8 and 10 in Table 3) have been selected to briefly describe the configuration variations of the PKM with different inputs (Fig.13).

It can be seen from Fig.13 that the length of the compliant joint has a significant effect on the performance of the system. Taking test 8 as an example, with the same input (i.e. the three SMA clutches having the same positions), the balanced configuration of the upper platform varies significantly (i.e. the average difference is 10.3 mm) with different lengths of the compliant joints. The reason for the position deviation of the upper platform can be attributed as: the static and kinematic performance of the limbs are sensitive/dependent with the length of the compliant joints, where the internal force distribution and stiffness is affected under different configurations of the P. Thus, the position and orientation of the upper platform satisfying (8) varies when different lengths of the compliant joints are utilised.

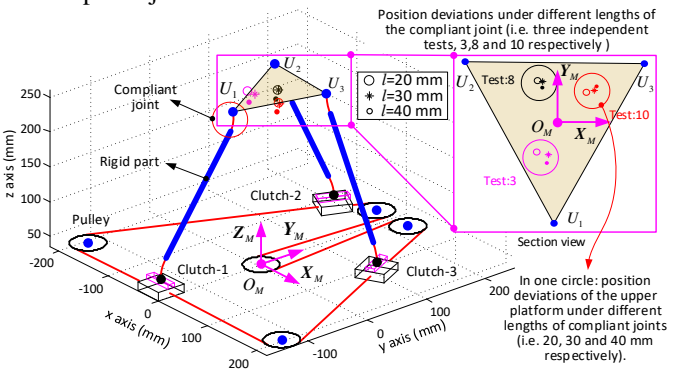

Fig.13. Schematic to explain the influence of the length of compliant joint (20, 30, 40mm) on the performance variation of the system (i.e. position and orientation deviations) using tests 3, 8, 10 as examples (Table 3). The positions of the upper platform under the specified experimental arrangements (i.e. number 3, 8 and 10 respectively) for different boundary directions are marked that correspond to different lengths of the compliant joint.

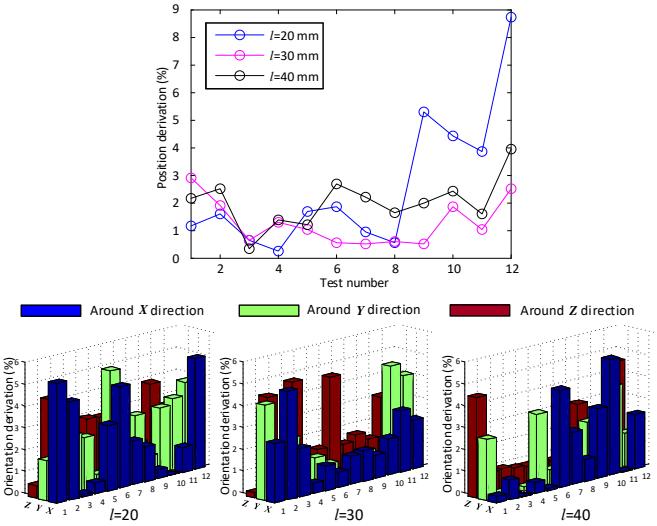

Fig.14. The position and orientation errors of the PKM under the given inputs of the three placing lines (Table 3). (a) error ($\sqrt{\Delta x^2+\Delta y^2+\Delta z^2}$) between the modelled and experimental position of the platform; (b) orientation errors of the upper platform (i.e. in $\boldsymbol{X}$, $\boldsymbol{Y}$ and $\boldsymbol{Z}$ directions respectively, defined in $\boldsymbol{ZYX}$ Euler angle) under the inputs shown in Table 3

Fig.14 (a) illustrates the overall position deviations of the upper platform under the given sets of inputs. It can be seen that the model presented in this paper can be validated with a

maximum deviation of 8.7% and an average deviation of 1.9% (i.e. the absolute errors are ±5.9 mm and ±2.6° in position and orientation respectively for the workspace (Fig.15)). In addition, the deviation of the upper platform when joint lengths are 30 and 40 mm are closing with each other, and they fluctuate between 0.2% and 3.8% respectively. However, for the compliant joint with the length of 20 mm, the deviations fluctuate similarly with 30 and 40 mm joint length from test 1 to 8, but then it quickly increases to around 4.2% afterwards, this is mainly due to the structure singularity in some specific configuration of PKM, causing the system instability.

Fig.14 (b) displays the orientation deviations of the upper platform for the given set of tests with different lengths of the compliant joints. It can be found (Fig.14) that the orientation deviations of the upper platform are within 6% during the tests. The average orientation deviations with three types of the complaint joint (i.e. l =20, 30 and 40 respectively) are 3.2%, 2.7% and 2.4% respectively, which proves the correctness of the model proposed in this paper.

C. *Workspace analysis*

Due to the introduction of the SCBDS in the overall system, it is becoming possible to use one motor to control the independent motion of three placing lines further, to control a 6-DoF PKM. However, this "advantage" in this mechanism will increase the motion variety of the upper platform, which raises the complexity of the workspace analysis.

Based on the motion characteristics of the proposed system (i.e. the three placing lines can only move to one direction at any time), the workspace of the system can be divided into two groups: one is the discrete workspace, which is generated by the discrete/random motions of the three placing lines; another is the continuous workspace that generated by the continuous motions of one, two or three placing lines simultaneously.

As the saw teeth have been adopted to increase the locking ability of the SMA clutch along each placing line (Fig.3), the locating position of each SMA clutch is not continuous anymore which results in the discretisation of the workspace of the system. Based on this observation, in the following, the workspaces have been evaluated by the designed characteristics of the placing lines (i.e. pitch of saw teeth of the moveable foot and base platform).

a) The discrete workspace of the system

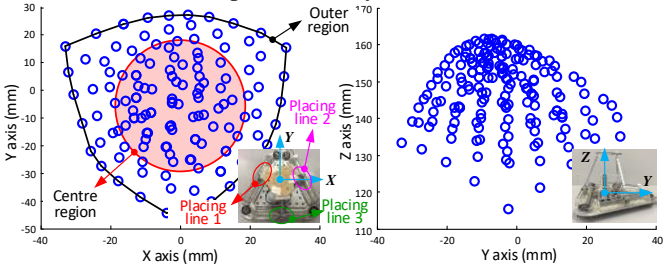

Fig.15. Examples of the discrete workspace of the under-actuated PKM with the given parameters of limbs (i.e. limb length: 180 mm, compliant joint length: 20 mm) in the condition of all three feet located randomly. a) Top view (from $\boldsymbol{Z}$ direction) of the workspace and (b) side view (from $\boldsymbol{X}$ direction) of the workspace respectively

This refers to the evaluation of workspace which is dependent on the location of the feet on the track (given "resolution" of the saw tooth indexing features) as well as on their movement direction along the placing lines. This was followed by the use of the kinetostatic model to obtain the poses of the upper platform of the manipulator.

The workspaces (Fig.15 with views from $\boldsymbol{Z}$ and $\boldsymbol{X}$ directions) are presented in the following conditions of the manipulator: (i) all three placing lines are located in random positioning; (ii) two of the placing lines (i.e. 2 and 3) are located randomly, while the remaining placing line (i.e. 1) keeps a fixed position.

It can be seen that the workspace of the proposed system is almost symmetrical, with respect to $\boldsymbol{Y}$ and $\boldsymbol{Z}$ axes (Fig.15). Nevertheless, this is dependent on the accuracy of the setup (e.g., the angle between the placing lines, relative positions between the saw tooth tracks, manufacturing errors, etc.). However, a very interesting point here is the resolution of positioning the centre point (O_U in Fig.8) of the platform is dependent on the resolution (i.e. pitch, Δ_l in Fig.3 (b)) of the saw teeth track. One reason is that the kinematic characteristics of the PKM (i.e., the relationship between the locations of three clutches and position of upper platform) are varying with different configurations of system; another reason is that the feet of the manipulator can be placed only in the positions that are defined by the conjugate profiles of the sawtooth features of the placing line and base platform. It can also be seen found that the position boundaries (mm) of the proposed PKM in $\boldsymbol{X}$, $\boldsymbol{Y}$ and $\boldsymbol{Z}$ directions are [-34, 34], [-47, 28] and [114, 162] respectively, while for the pose boundaries (degree) in $\boldsymbol{X}$, $\boldsymbol{Y}$ directions are within [-19, 19], for $\boldsymbol{Z}$ direction is within [-37, 37].

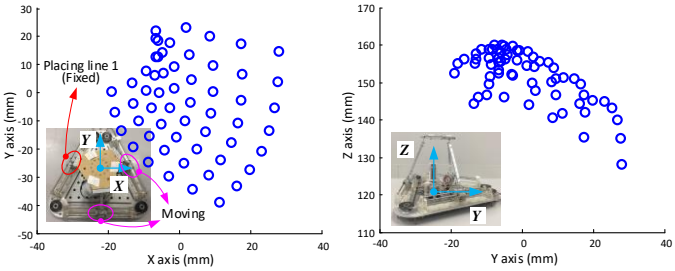

Fig.16. Examples of the discrete workspace of the system with placing lines 2 and 3 randomly moving within their strokes, while the placing line 1 is fixed. (a) and (b) are the top view and (b) side view of the workspace respectively

By this inference, the system resolution, Δ_o, can be calculated from (8) to (13) by inputting the position of the feet and the value of the resolution, Δ_l, of the saw tooth tracks. This leads to the notable observation that the resolution of the centre point of the manipulator, Δ_i, being of lower value (average 0.35 mm) in the centre region of the workspace and of higher value (average 0.68 mm) at its outer region (see notations in Fig.15).

Fig.16 is the workspace of the system with two placing lines (i.e. 2 and 3) moving along their guides while placing line 1 is fixed at the middle of its stroke.

As expected, the workspace captures only one section of the full workspace while the distance between the positions of the centre point of the upper platform is not uniform although the placing lines have been moved with the same increment, i.e. smaller distances towards the centre of the work volume (see Fig.16). Interesting to note that a position of the upper platform can be achieved by moving all placing lines (case (i)) or keeping one at a fixed position and moving only two placing line (case (ii)) but at a higher resolution in the last case. It could be commented that the discrete workspace is of relevance for pick-and-place manipulators where discrete positions of the platform are sufficient to satisfy the engineering applications.

b) The continuous workspace of the system

In this case, one, two or all (three) placing lines move continuously and in the same direction (imposed by the movement of the driving cable). Interesting to observe that under these restrictions, the "workspaces" become families of moving curves in a 3D space. Of course, the resolution of positioning the upper platform along the moving curves is dependent on the resolution of the linear encoders, but in a full

3D (spacing between the moving curves) it depends again on the resolution of the saw teeth, Δ_l.

Thus, based on the working principle of the SMA clutch-based driving system, the motion characteristics of the placing lines can be divided into the following three cases. Case 1: one of the placing lines moves within the stroke, while the rest two placing lines remain stationary; Case 2: two of the placing lines move within their strokes at the same speed and direction, but the third one remains stationary; Case 3: three placing lines move at the same speed and direction to actuate the PKM. The workspaces for all of the three cases are plotted in Fig.17. The resolution of the system was studied, which is the displacement of the upper platform when the placing lines move with a minimal move one pitch (1.5 mm – saw teeth width of the placing line).

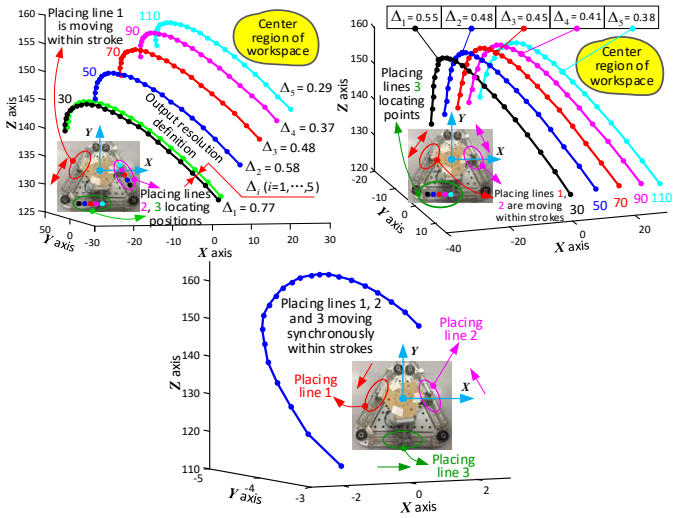

Fig.17. Continuous workspace of the proposed PKM under Case 1, 2 and 3 (the curves represent the positions of the moving platform when the placing lines are at different positions of their strokes. a) Case 1 - placing line 1 moves continuously at the same direction while placing lines 2 and 3 are fixed at different locations within their strokes; b) Case 2 - placing line 1 and 2 move continuously while placing line 3 is clamped at different locations within its stroke; c) Case 3 – all three lines move simultaneously within their strokes.

In this analysis, all the fixed placing lines start to be placed at the location of 30 mm from one end of their strokes and move toward the other end with an increment displacement of 1.5 mm (the pitch of the placing lines). Fig.17 presents the workspace of the system when the fixed placing lines are positioned at the locations of 30mm, 50mm, 70mm, 90mm and 110mm, respectively (case 1 – line 2 and 3; case 2 – line 3). Although the feet moved with identical increment, it can be seen that the resolution of the system (Δ_i) varies in the entire workspace when the system takes different configurations; see the change of the value Δ_i in Fig.17 (a) and (b). In case 1 (Fig.17 (a)), the value of the resolution of the system decreases from the border to the centre regions of the workspace. Specifically, resolutions Δ_1 to Δ_5 are 0.77 mm, 0.58 mm, 0.48 mm, 0.37 mm and 0.29 mm, when the fixed placing lines are at the locations of 30mm, 50mm, 70mm, 90mm and 110mm, respectively. The same tendency was also found in the discrete workspace study (Fig.15 (a)). In Fig.17 (b), a similar result was identified; the resolution of the family curves decrease (i.e., Δ_1: 0.55 mm, Δ_2: 0.48 mm, Δ_3: 0.45 mm, Δ_4: 0.41 mm and Δ_5: 0.38 mm, respectively) from the border to the centre of the workspace. In case 3, all the placing lines move simultaneously from one end of their strokes to the other one. Hence, just one continuous curve of the upper platform position can be generated. In this case, the upper platform has small movements in ***X*** and ***Y*** directions, which is close to a circular arc shape (i.e. centre: around [0, 0], radius: 4 mm), while the height of the upper platform has a big variation (from 115.3 mm at the beginning to 160.8 mm at the middle, and then drop to 148 mm at the end).

From all these results, it can also be found that, by inputting a unit displacement from the actuation, the upper platform can move faster in the outer region of the workspace, while slower in the centre area. This is an interesting observation that enables the operator to use different regions of the system workspace for distinct operations (e.g., slow and fine manipulations in the centre region of the workspace, while fast and course manoeuvrings in the outer area).

In this section, the experimental validation for the proposed kinetostatic modelling was conducted on the proposed PKM. By varying the locations of all three SMA clutches, the configurations of the upper platform (i.e. position and orientation) were calculated and measured respectively. It could be observed that the proposed kinetostatic models have been proved accurate (i.e. overall position deviation 1.8% and orientation deviation 2.8% respectively). Then, with the validated kinetostatic model developed in this paper, the workspace of the PKM was studied, which is important for understanding how the movements of the placing lines influence the movement of the upper platform of the under-actuated PKM. After studying the discrete (i.e. three placing lines move independently to achieve the maximum workspace of the system) and a continuous workspace of the system, the resolution variation of the system was studied under the different working characteristic of placing lines. It was found that the resolution of the PKM is unevenly distributed among the workspace (i.e. higher resolution within the centre region of the workspace, 0.35 mm, and lower resolution in the outer region of workspace, 0.68 mm).

V. Conclusions

In this paper, a novel under-actuated 6-DoF PKM, which uses a drive cable in combination with smart shape memory alloy (SMA) clutches, three stiffness-adjustable limbs and an upper platform, was proposed to perform a multiple-degrees operation with a single actuator. Based on the proposed manipulator, the novelties can be summarized as follows.

Firstly, an advanced compliant parallel mechanism, in which conventional rigid joints were replaced with stiffness-adjustable joints, has been developed to allow the safe human-robotic interaction. To achieve this, super-elastic NiTi rods were selected to generate the motions (i.e. by material deformation) as conventional rigid joints. Further, in order to actively control the stiffness of the system, the length of the compliant joints was designed to be adjustable, which was operated by covering the NiTi alloy rod with a set of small fixed-length rigid segments. Hence, in this paper, a traditional universal/spherical joint-based PKM with complicated structure and strict assembling requirements have been transferred to a novel PKM.

Further, a novel cable-driven SMA clutch-based driving system has been developed for actuating the parallel manipulators with a reduced number of actuators (i.e. using a single actuator to control a 6-DoF manipulator), which provides a new way for actuating, in a simple and efficient way, multiple-DoF parallel manipulators only with one motor. Furthermore, an SMA wire-based clutch (characteristics: small size, powerful output and quick response) that enables the under-actuation of the manipulator has been demonstrated; it's simple but efficient design is a viable alternative to bulky conventional (e.g. electromagnetic) clutches.

In addition, for studying the kinematic characteristics (i.e. positioning and orientation accuracy) of the proposed under-actuated system, a novel kinetostatic model was developed to predict the performances of an end-effector by considering the external and internal loads. Specifically, by accounting for the bending and torsion characteristics of each compliant joint and force and moment of the upper platform, the generated forces and moments in three limbs have been calculated to establish the overall static equation of the upper platform. Based on the proposed models, the outputs of the system (i.e. position and orientation of the upper platform) can be predicted with the given inputs of the system (i.e. positions of three SMA clutches). Then, the validation process was conducted based on the proposed prototype (i.e. a triple manipulator) and its control system which yielded average deviations 1.8% in position and 2.8% in orientation (Fig.14). The analysis of discrete and continuous workspaces indicates that the proposed parallel mechanism (i.e. structured by three limbs) can be used as a 6-DoF manipulator with only one motor as the actuator. It was also found that the resolution of the system is unevenly distributed within the workspace, i.e. higher in the centre region (0.35 mm), lower in the outer region (0.68 mm) which mainly depends on the pitch of the saw-tooth features of the clutches (see Fig.3). Hence, for operations with distinct movement requirements (e.g. fine positioning - assembly of small components; course positioning - pick and place in logistic lines), the system design could be customized for different regions of the workspace, in order to optimize the manipulation time and energy consumption.

VI. ACKNOWLEDGE

The research leading to these results has received funding from the China Scholarship Council, University of Nottingham, EPSRC projects (EP/P027121/1 Through-life performance: From science to instrumentation and EP/R026084/1 Robotics and Artificial Intelligence for Nuclear).

REFERENCES

[1] Jani, Jaronie Mohd, et al. "A review of shape memory alloy research, applications and opportunities." Materials & Design (1980-2015) 56 (2014): 1078-1113.
[2] Sun, Li, et al. "Stimulus-responsive shape memory materials: a review." Materials & Design 33 (2012): 577-640.
[3] Zhu, Xiaocong, et al. "Adaptive robust posture control of parallel manipulator driven by." IEEE-ASME T MECH 13.4 (2008): 441-450.
[4] Fang, Shiqing, et al. "Motion control of a tendon-based parallel manipulator using optimal distribution." IEEE-ASME T MECH 9.3 (2004): 561-568.
[5] Palpacelli, Matteo-Claudio, et al. "Analysis and design of a reconfigurable 3-DoF parallel manipulator." IEEE-ASME T MECH 20.4 (2014): 1975-1985.
[6] Laski P A, Takosoglu J E, Blasiak S. Design of a 3-DOF tripod electro-pneumatic parallel manipulator[J]. ROBOT AUTON SYST, 2015, 72: 59-70.
[7] Zi B, Sun H, Zhang D. Design, analysis and control of a winding hybrid-driven cable manipulator[J]. ROBOT CIM-INT MANUF, 2017, 48: 196-208.
[8] Andrew L. Orekhov, Caroline B. al. Analysis of a teleoperated surgical parallel manipulator[J]. IEEE Robot Autom Lett. 2016. 1（2）: 828-835
[9] Xin Dong, D. Axinte, David Palmeret al. Development of a slender continuum robotic system for on-wing inspection/repair of gas turbine engines[J]. ROBOT CIM-INT MANUF. 2017. 44: 218-229
[10] Dragos Axinte, Xin Dong, David Palmeret al. MiRoR—Miniaturized Robotic Systems for In-Situ Repair and Maintenance Works in Restrained and Hazardous Environments[J]. IEEE-ASME T MECH. 2018. 23 (2): 978-981
[11] Renda, Federico, et al. "Dynamic model of a multibending soft robot arm driven by cables." IEEE Transactions on Robotics 30.5 (2014): 1109-1122.
[12] Carmel Majidi. Soft robotics: a perspective—current trends and prospects for the future[J]. Soft Robotics. 2014. 1 (1): 5-11
[13] Minh Tuan Pham, Tat Joo Teo al. A 3-D Printed Ti-6Al-4V 3-DOF Compliant Parallel Mechanism for High Precision Manipulation[J]. IEEE-ASME T MECH. 2017. 22 (5): 2359-2368
[14] Qiaokang Liang, Dan Zhang, Zhongzhe Chiet al. Six-DOF micro-manipulator based on compliant parallel mechanism with integrated force sensor[J]. ROBOT CIM-INT MANUF. 2011. 27 (1): 124-134
[15] John Till, D. Caleb Rucker. Elastic stability of Cosserat rods and parallel continuum robots[J]. IEEE Transactions on Robotics. 2017. 33 (3): 718-733
[16] Caroline B. Black, John Till, D. Caleb Rucker. Parallel Continuum Robots: Modeling, Analysis Force Sensing[J]. IEEE T ROBOT. 2018. 34 (1): 29-47
[17] Jonathan B. Hopkins al. Synthesis and analysis of soft parallel robots comprised of active constraints[J]. IEEE T ROBOT. 2015. 7 (1): 11002
[18] Yang, Chifu, et al. "PD control with gravity compensation for hydraulic 6-DOF manipulator." Mechanism and Machine theory 45.4 (2010): 666-677.
[19] Marco Salerno, Amir Firouzeh. A low profile electromagnetic actuator design for an origami parallel platform[J]. J MECH ROBOT. 2017. 9 (4): 41005
[20] Wei Dong, L. N. Sun, Z. J. Du. Design of a precision compliant parallel positioner driven by dual piezoelectric actuators[J]. SENSOR ACTUAT A-PHYS. 2007. 135 (1): 250-256
[21] Arne O Lander. An electrochemical investigation of solid cadmium-gold alloys[J]. Journal of the American Chemical Society. 1932. 54 (10): 3819-3833
[22] Julian Colorado, Antonio Barrientos, Claudio Rossiet al. Biomechanics of smart wings in a bat robot: morphing wings using SMA actuators[J]. Bioinspiration \& biomimetics. 2012. 7 (3): 36006
[23] Byungkyu Kim, Sunghak Lee al. Design and fabrication of a locomotive mechanism for capsule-type endoscopes using shape memory alloys (SMAs)[J]. IEEE-ASME T MECH. 2005. 10 (1): 77-86
[24] Zhao Guo, Yongping Pan, Liang Boon Weeet al. Design and control of a novel compliant differential shape memory alloy actuator[J]. Sensors and Actuators A: Physical. 2015. 225: 71-80
[25] Jeremy Kolansky, Pablo Tarazaga, O. John Ohanian. Experimental Implementation of Opposed Shape Memory Alloy Wires for Actuator Control[J]. Journal of Vibration and Acoustics. 2015. 137 (1): 11007
[26] Hashem Ashrafiuon, Mojtaba Eshraghi, Mohammad H. Elahinia. Position control of a three-link shape memory alloy actuated robot[J]. Journal of intelligent material systems and structures. 2006. 17 (5): 381-392
[27] Kai Xu, Nabil Simaan. An investigation of the intrinsic force sensing capabilities of continuum robots[J]. IEEE T ROBOT. 2008. 24 (3): 576-587
[28] D. Caleb Rucker, Bryan A. Jones, Robert J. Webster III. A geometrically exact model for externally loaded concentric-tube continuum robots[J]. IEEE transactions on robotics. 2010. 26 (5): 769
[29] Pierre E. Dupont, Jesse Lock, Brandon. Design and control of concentric-tube robots[J]. IEEE Transactions on Robotics. 2010. 26 (2): 209-225
[30] Caroline E. Bryson, D. Caleb Rucker. Toward parallel continuum manipulators[M]IEEE，2014: 778-785
[31] Larry L. Howell, Ashok Midha, T. W. Norton. Evaluation of equivalent spring for use in a pseudo-rigid-body model of large-deflection compliant mechanisms[J]. Journal of Mechanical Design. 1996. 118 (1): 126-131
[32] Ashok Midha, Larry L. Howell, Tony W. Norton. Limit positions of compliant mechanisms using the pseudo-rigid-body model concept[J]. Mechanism and Machine Theory. 2000. 35 (1): 99-115
[33] Nan Ma, Jingjun Yu, Xin Donget al. Design and stiffness analysis of a class of 2-DoF tendon driven parallel kinematics mechanism[J]. Mechanism and Machine Theory. 2018. 129: 202-217
[34] Guang Yu, Liping Wang, Jun Wuet al. Stiffness modeling approach for a 3-DOF parallel manipulator with consideration of nonlinear joint stiffness[J]. Mechanism and Machine Theory. 2018. 123: 137-152
[35] Yu, J. J., et al. "Mobility and singularity analysis of a class of 2-DOF rotational parallel mechanisms using a visual graphic approach." ASME 2011 international design engineering technical conferences and computers and information in engineering conference. American Society of Mechanical Engineers Digital Collection, 2011.

Nan Ma is a research fellow of University of Nottingham, working at the Department of Mechanical Materials and Manufacturing Engineering. His research interests are design, static and dynamic analysis of parallel mechanisms (i.e. walking and flying robots). He is also doing the soft material-based robotics, such as continuum and stiffening robots.

Xin Dong is the assistant professor working at the University of Nottingham. His research interests are extra slender continuum robot and reconfigurable hexapod robots with novel actuation solutions for the application in Aerospace, Nuclear, Oil&Gas, Marine and rescue.

Dragos Axinte is Fellow of the Institution of Mechanical Engineer (IMechE) and Fellow of the International Academy of Production Engineering (FCIRP). Since 2009 he is the Director of the Rolls-Royce University Technology Centre (UTC) in Manufacturing and On-Wing Technology. He is also Editor-in-Chief of the International Journal of Machine Tools and Manufacture